Geoderma 321 (2018) 127–140

Contents lists available at ScienceDirect

Geoderma

journal homepage: www.elsevier.com/locate/geoderma

Geochemical characterization of the loess-paleosol sequence in northeast China

Zhong-Xiu Sun[a,1], Ying-Ying Jiang[a,1], Qiu-Bing Wang[a,*], Phillip Ray Owens[b,**]

[a] College of Land and Environment, Shenyang Agricultural University, Shenyang, Liaoning Province 110866, China.
[b] Dale Bumpers Small Farms Research Center, Booneville AR72927, USA.

ARTICLE INFO

Handling Editor: Dr. M. Vepraskas

Keywords:
Elemental geochemistry
Weathering history
Pedogenesis

ABSTRACT

Long-term weathering patterns in northeastern China are not well known due to few well-preserved terrestrial paleo-environmental archives in this area. The Chaoyang section is a typical well-preserved loess-paleosol sequence in northeast China with continuous deposition since 423 ka BP; the deposit thus represents an archive of climate change for this region. The sequence was geochemically characterized by major elemental compositions, elemental ratios, a ternary diagram of Al_2O_3-(CaO* + Na_2O)-K_2O, improved quantitative reconstruction and elemental distributions with respect to the average for the upper continental crust (AUCC). Another typical loess-paleosol sequence of Lingtai section from the central Chinese Loess Plateau was used for comparison with the loess-paleosol one. The similar AUCC-normalized major elemental distributions and strong correlation of the major elemental compositions between the loess-paleosol sequences indicate that they may have originated predominantly from a similar loess source. Based on the variability in chemical indices corresponding to soil magnetic susceptibility (SUS) and field observations, the loess-paleosol formation period of 423–77 ka BP was separated into eight sub-periods including four periods with greater chemical weathering intensity (paleosols) and four periods characterized by the relative lesser chemical weathering intensity (loess). Relatively intense desilication and fersiallitization primarily occurred in the loess-paleosol sequence from northeast China with greater losses of SiO_2 (3.54% in average) and gains of Fe_2O_3 (0.77%) and Al_2O_3 (0.33%). Such processes also were reflected in an increase in the amount of K_2O (0.41%). Ca and Na leaching was still predominant in the loess-paleosol sequence from the central Chinese Loess Plateau with greater losses of CaO (28.03%) and Na_2O (14.03%). The sequence from northeast China records chemical weathering during 423–77 ka BP, which is comparable to the weathering cycles in the sequence from the central Chinese Loess Plateau.

1. Introduction

1.1. Research significance

Weathering can alter soils in terms of micro-fabric, mineralogical, and geochemical features. Objective and quantitative evaluation of weathering-induced changes are important for aiding the interpretation of environmental changes. The Quaternary loess-paleosol sequence records the long-term chemical weathering history (Yang et al., 2006) and can reflect land surface stability and Pleistocene climatic evolution (Buggle et al., 2011). The long-term weathering history and climatic evolution of northeastern China is not well known due to few well-preserved terrestrial paleo-environmental records in this area.

1.2. Development of geochemical proxies of weathering

Relative geochemical changes between mobile and immobile elements can be used to evaluate weathering-induced changes (Mason and Moore, 1985; Schaetzl and Anderson, 2005; Yang et al., 2006). More than 30 chemical weathering indices have been proposed since the beginning of the 20th century (Duzgoren-Aydin et al., 2002) to indicate mineral weathering and elemental migration in different sediments such as loess and paleosol sequences. These indices are reviewed in detail by Duzgoren-Aydin et al. (2002). Buggle et al. (2011) evaluate their suitability for investigating loess-paleosol sequences. Other possibilities are a Sr weathering index, e.g. Rb/Sr (Chen et al., 1999; Tan et al., 2006), a Ba/Sr index though (Bokhorst et al., 2009) this may be affected by secondary carbonate due to a possible substitution of Ca by

* Corresponding author at: No. 120 Dongling Road, Shenhe District, College of Land and Environment, Shenyang Agricultural University, Shenyang, Liaoning Province 110866, China.
** Corresponding author.
E-mail addresses: wangqbsy@yahoo.com (Q.-B. Wang), Phillip.Owens@ars.usda.gov (P.R. Owens).
[1] Both authors contributed equally to this work and should be considered co-first authors.

https://doi.org/10.1016/j.geoderma.2018.02.012
Received 14 March 2017; Received in revised form 24 January 2018; Accepted 4 February 2018
Available online 20 February 2018
0016-7061/

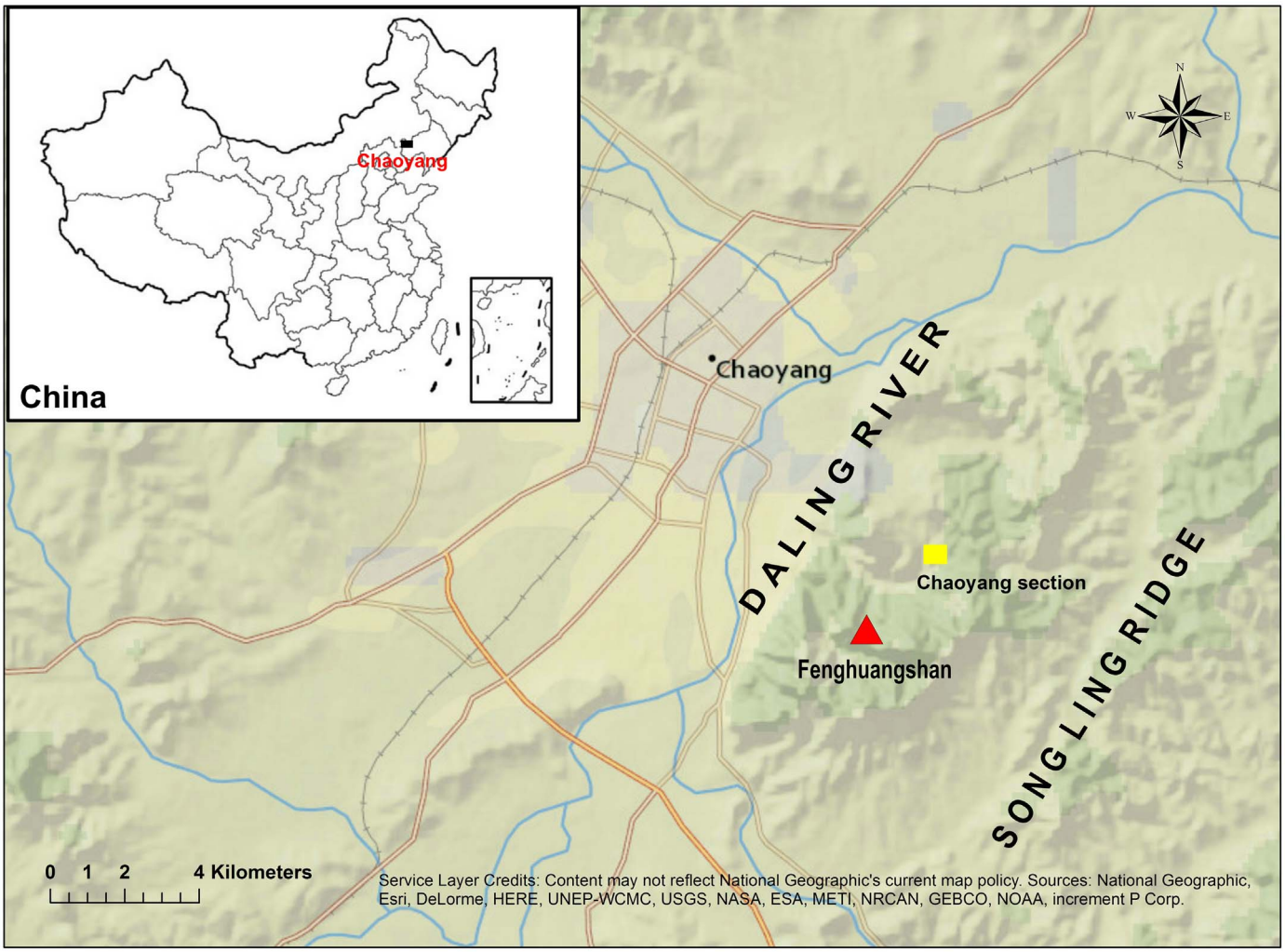

Fig. 1. Schematic map presenting the location of Chaoyang loess-paleosol section (Sun et al., 2016). The black square on the inset map shows the location of Chaoyang in China. The schematic map was plotted basing on the base map of National Geographic World Map (2010) using Arc GIS 10.2.2.

Sr (Buggle et al., 2011). Such an index should be restricted to carbonate-free sediments (Dasch, 1969; Nesbitt and Markovics, 1980). The Na associated weathering index (e.g. CIA, CIW) is likely to be influenced by uncertainties from the correction for CaO* in silicate minerals (Buggle et al., 2011). Na_2O/Al_2O_3 (Gu et al., 1999), the Chemical Index of Alteration (CIA) (Liu et al., 1995; Nesbitt and Young, 1982), the Chemical Index of Weathering (CIW) (Harnois, 1988), and a proxy, free of grain-size effects of Loess Weathering Index (LWI) (Yang et al., 2006), the Plagioclase Index (PIA) (Fedo et al., 1995), the Weathering Index of Parker (WIP) (Parker, 1970), Chemical Proxy of Alteration (CPA) (Buggle et al., 2011) and Index B (Kronberg and Nesbitt, 1981) have all been widely used in evaluating the loess-paleosol chemical weathering (Buggle et al., 2011; Ding et al., 2001; Gallet et al., 1996; Guo et al., 2000; Liu, 1985; Schellenberger and Veit, 2006; Yang et al., 2006). The CPA is considered by Buggle et al. (2011) as the most appropriate geochemical proxy, excluding CaO* (free of CaO* related uncertainties) and K_2O (free of K inconsistent behavior by K-fixation (Harnois, 1988)). It can be used for indicators of loess-paleosol weathering which can indicate feldspar (especially plagioclase) weathering in a loess-paleosol sequence. As soil weathering changes depend on environmental conditions (Roy et al., 2012), geochemical proxies containing information on the soil weathering intensity can be valuable indicators for reconstructing paleoclimatic conditions (Buggle et al., 2008; Sheldon et al., 2002).

1.3. Mass balance interpretation

A loess-paleosol sequence has unique pedogenesis in that pedogenic processes are synchronized with loess deposition (Sun et al., 2016). The loess may have been partly influenced by elemental translocations from the overlying layers, which may mask the geochemical signals. It is also difficult to estimate elemental migration within the loess deposits. Insoluble hydrolyzates such as Ti and Zr are often used as references to reveal possible elemental translocations (Brewer, 1976; Egli et al., 2001). As the former can be easily analyzed together with major elemental composition, the use of Ti is commonly employed. The method of Gallet et al. (1996) has been widely used to estimate the relative elemental changes between loess and a paleosol (Yang et al., 2006). In this method the loess elemental composition is assumed to be the initial elemental composition for the overlying paleosol. If this method is employed, the weathering history cannot be fully addressed due to the assumption of un-weathered loess (weak developed loess in fact). On the other hand, the loess has undergone to some extent of weathering rather than un-weathered, which is not appropriate to be selected as the initial for the overlying paleosol. There are advantages in selecting an assumed parent material for a loess-paleosol sequence proposed by Brewer (1976). The deepest loess layer, with the least weathering intensity and uniform elemental distribution, especially Ti and Zr, should be assumed as the parent material for a loess-paleosol sequence. Therefore, the method of Gallet et al. (1996) has been revised and

summarized in this paper (see Section 2.4.).

The Chaoyang section is a key well-preserved loess-paleosol sequence in northeast China, where loess has been continuously deposited since 423 ka BP, and provides a record of climate change in this region (Chen et al., 2009; Sun et al., 2016; Sun et al., 2016). Elemental compositions are widely used as weathering indices for loess-paleosol sequences together with the revised reconstruction method of Gallet et al. (1996). The elemental losses and gains were evaluated to address the weathering history in northeast China during 423–77 ka BP.

2. Materials and methods

2.1. Environmental setting and sampling

A typical loess-paleosol sequence in northeast China is the Chaoyang section (Chen, 2009; Sun et al., 2016) located at Chaoyang (N 41°33′9.6″, E 120°30′ 20.8″), which is beyond the northeast corner of the Chinese Loess Plateau (Fig. 1). The present-day average annual precipitation and average annual temperature are 450–500 mm and 9 °C in Chaoyang, respectively. The soil (the Holocene soil, S0) is Cinnamon one which is classified as Haplustalfs according to the US Soil Taxonomy (Soil Survey Staff, 2014). The section consists of five loess units (Lx) and four intervening paleosols (Sx), with 42 genetic horizons (Sun et al., 2016). The detailed morphological features were described in the field (Sun et al., 2016).

Forty-two samples from the horizons were collected from the bottom (L5) to the top (S0). Around 5 kg of soil material was collected per soil horizon. Undisturbed soil samples were taken down to 1985 cm. The section, except for evidence of local reworked loess above 228 cm, was derived from eolian loess, and had been deposited continuously since 423 ka BP (Chen et al., 2009; Sun et al., 2016). Due to the presence of mixed material above 228 cm, this research focuses on the uniform lower part of the Chaoyang section (LOP) below 228 cm. Some basic properties of LOP are listed in Table 1. L5 has been demonstrated that it can be selected as a reference (Sun et al., 2016) and is assumed to represent the parent material for LOP in this research. The chronostratigraphy of the Chaoyang section was cited from Chen et al. (2009) and Sun et al. (2016).

Another typical loess-paleosol sequence is the Lingtai section (N 35°00′, E 107°30′) (Ding et al., 2001), located in the central Chinese Loess Plateau, about 1334 km southwest from the Chaoyang section. The present mean annual precipitation and mean annual temperature is 600 mm and 8.6 °C, respectively. The details of the stratigraphy and time scale are given by Ding et al. (2001). Only the loess-paleosol sequence of 423–77 ka BP in the Lingtai section was compared to the Chaoyang section.

2.2. Analytical methods

Soil bulk density measurements of each horizon were determined using the clod method (Brasher et al., 1966). Soil pH of each horizon was measured on air-dried samples (< 2 mm) using a soil/deionised water solution ratio of 1:2.5. Concentrations of K, Na, Ca, Mg, Al, Fe, Mn, Si and Ti were determined by X-ray Fluorescence Spectrophotometer (XRF) using the method of Cesareo (2010). Loss on ignition was determined by heating an aliquot of the sample at 950 °C for one hour. Two standard soil samples of GBW(E)-070041 and GBW(E)-070042 in China, were added and measured synchronously to monitor the quality of analysis. Results of elemental compositions were calculated and presented as percent oxide, and had relative errors < 5% and the standard deviation of one randomly selected sample in triplicate was < 3%.

2.3. Elemental ratios used to quantify the chemical weathering intensity of the loess-paleosol sequence

Widely used elemental molar ratios (Table 2) in loess research include Na_2O/Al_2O_3 (Gu et al., 1999), K_2O/Al_2O_3 (Garrels and Mackenzie, 1971), Na_2O/K_2O (Li et al., 2007), the Chemical Index of Alteration (CIA) (Liu et al., 1995; Nesbitt and Young, 1982), the Chemical Index of Weathering (CIW) (Harnois, 1988), and a proxy, free of grain-size effects of Loess Weathering Index (LWI) (Yang et al., 2006) are employed in this paper to quantify the chemical weathering intensity of loess-paleosol in the Chaoyang section. In addition, the Plagioclase Index (PIA) (Fedo et al., 1995), the Weathering Index of Parker (WIP) (Parker, 1970) and the Chemical Proxy of Alteration (CPA) (Buggle et al., 2011) are also used to better evaluate the degree of loess-paleosol chemical weathering. These index formulas are summarized in Table 2 and their detailed definitions can be found in corresponding references.

The CaO* in Table 2 denotes the CaO content in silicate-bearing minerals only (Nesbitt and Young, 1982). The measured CaO content data by XRF was approximately corrected to exclude the Ca content in phosphates (apatite) and carbonates (calcite and dolomite) using the method of McLennan (1993). First, the measured molar CaO content was corrected for Ca in apatite using the available measured P_2O_5 content. In general, the molar ratio of CaO/Na_2O is assumed to be not greater than that in the silicate material. Then, if the remaining mole of CaO content (corrected for apatite) is greater than Na_2O, the $mCaO^* = mNa_2O$ (the molar content) was adopted. In contrast, if the remaining mole of CaO content was less than that of Na_2O, $mCaO^* = mCaO$ was used (McLennan, 1993).

The WIP index was first proposed by Parker (1970) and is expressed as atomic proportions of certain mobile elements (Table 2) which include consideration of the necessary energy to break bonds (Nicholls, 1963) between the cation and oxygen in oxides. The bond strength can reflect the probability of an element being mobilized during weathering (Bahlburg and Dobrzinski, 2011). The WIP index ranges from 0 to 100. Greater values of WIP indicate smaller weathering intensity. The disadvantage of the WIP index is the lack of a relatively immobile reference to monitor relevant mineral changes (Bahlburg and Dobrzinski, 2011).

The WIP index includes all Ca in the silicate minerals. The CIA index includes major elemental oxide data and CaO in the silicate-bearing minerals only. This can overcome the disadvantage of the WIP index. CIA can quantitatively measure the silicate weathering extent in terms of progressive alteration of plagioclase and K-feldspars to clay minerals using the proportion of Al_2O_3 versus labile oxides (Nesbitt and Young, 1982). Al should be rich in the weathering residues, and the removal of K, Na and Ca from a soil profile should occur due to plagioclase and K-feldspar weathering. CIA values of 45–55 indicate virtually no weathering, and 100 represents extreme weathering with removal of all the alkali and alkaline (McLennan, 1993). Fedo et al. (1995) classified the soil weathering intensity using CIA values as incipient (50–60), intermediate (60–80) and extreme weathering (> 80). The average upper continental crust (AUCC) (Hawkesworth and Kemp, 2006) has a CIA value of 52.74 (Rudnick and Gao, 2003). Therefore, CIA values of < 55 are regarded as displaying no weathering and 55–60 as incipient weathering.

The PIA index can be used to monitor plagioclase weathering whose equation is modified from CIA equation (Fedo et al., 1995). The PIA values are consistent with the CIA ones.

Compared to the CIA index, the CIW index excludes potassium which may be leached or accumulated in the residue during weathering (Harnois, 1988). The CIW index value, as an indicator of the soil depletion degree in Na_2O and CaO relative to Al_2O_3, increases with the soil weathering intensity.

The LWI was proposed and reported by Yang et al. (2006) to be a good proxy for accessing chemical weathering intensity in the loess-

Table 1
Basic soil morphologic properties of the LOP in the Chaoyang section[a].

Stratum	Horizon	Depth (cm)	Age (ka BP)	Color (dry)	Texture	Structure	Consistence (dry)	Clay films	pH	BD[b] g/cm^3
S1–2	3Btb1	228–301	89.60	2.5YR 6/6	SI	2, CO, SBK	EH	3kpf	8.47	1.50
	3Btb2	301–391	106.00	2.5YR 5/6	SI	2, M, SBK-ABK	EH	4kpf	8.38	1.53
	3Btb3	391–462	118.40	2.5YR 5/6	SI	2, m, SBK-ABK	MH	4kpf	7.83	1.45
	3Btb4	462–587	140.70	2.5YR 6/6	SI	2, CO, SBK-ABK	MH	4kpf	7.75	1.38
	3Btb5	587–630	148.00	2.5YR 6/6	SI	2, VC, SBK	VH	4kpf	7.38	1.57
	3Btb6	630–690	155.30	2.5YR 6/6	SI	2, VC, SBK	VH	4kpf	7.38	1.57
	3Btb7	690–719	159.00	5YR 6/6	SI	2, VC, SBK	EH	4mkpf	7.35	1.43
L2	4Btb1	719–746	162.10	5YR 6/6	SI	1, M, SBK	EH	4npf	7.39	1.49
	4Btb2	746–858	175.80	5YR 6/6	SI	1, M, SBK	MH	4npf,4npo	7.41	1.40
S2	5CBtb	858–952	208.00	5YR 6/6	SI	1, M, SBK-ABK	VH	v1mkpo,v1mkpf	7.77	1.39
L3	6Ab	952–971	210.50	7.5YR 7/6	SI	1, M, SBK	VH	v1npo	7.90	1.56
	6Btb	971–1061	221.50	7.5YR 7/6	SI	1, CO, SBK	EH	3npo,3npf	7.91	1.59
	6CBb	1061–1090	225.00	5YR 6/6	SI	1, M, SBK	EH	v1npo	7.95	1.54
S3	7Btb	1090–1169	243.00	2.5YR 5/8	SI	2, m, sbk	MH	4kpf,4kpo	7.90	1.32
L4	8Ab	1169–1192	248.00	5YR 6/6	SI	1, F, SBK-ABK	MH	1npo	7.87	1.58
	8Btb1	1192–1214	253.00	7.5YR 6/6	SI	1, F, SBK-ABK	MH	v1npo,v1npf	7.81	1.51
	8Btb2	1214–1236	258.10	7.5YR 6/6	SI	1, F, SBK-ABK	VH	v1npo,v1npf	7.83	1.53
	8Btb3	1236–1259	263.50	5YR 7/4	SI	2, CO, SBK-ABK	MH	v1npo,v1npf	7.75	1.50
	8CBb1	1259–1308	274.50	7.5YR 7/6	SI	1, VC, SBK	HA	v1npo	7.85	1.52
	8CBb2	1308–1367	288.20	7.5YR 8/4	SI	1, CO, ABK-PR	EH	v1npo	7.74	1.49
	8CBb3	1367–1389	293.20	7.5YR 8/3	SIL	1, CO, ABK	HA	v1npo	7.77	1.32
	8CBb4	1389–1410	297.80	7.5YR 8/3	SI	1, CO, PR-ABK	HA	v1npo	7.84	1.46
	8CBb5	1410–1431	302.80	7.5YR 8/4	SI	1, CO, PR-ABK	HA	v1npo	7.82	1.39
	8CBb6	1431–1466	310.50	7.5YR 8/4	SI	1, M, ABK	HA	v1npo	7.84	1.36
S4	9Ab	1466–1526	323.70	7.5YR 7/6	SI	1, CO, SBK	EH	1npo	7.58	1.39
	9Btb1	1526–1556	330.30	5YR 6/6	SI	1, CO, SBK	EH	1npo	7.63	1.39
	9Btb2	1556–1612	342.50	5YR 6/6	SI	1, VC, SBK	MH	1npo	7.77	1.45
	9Btb3	1612–1643	349.60	5YR 6/6	SI	1, M, SBK	MH	1npo	7.76	1.41
	9Btb4	1643–1715	365.80	5YR 6/6	SI	2, M, SBK-ABK	MH	4kpf	7.69	1.46
	9Btb5	1715–1765	376.70	2.5YR 6/8	SI	2, M, SBK	MH	4kpf	7.81	1.46
	9Btb6	1765–1846	381.50	2.5YR 5/6	SI	1, CV, SBK	EH	4kpf	7.88	1.46
	9BCtb	1846–1885	403.00	5YR 5/6	SI	1, VC, SBK	EH	4kpf	7.96	1.46
L5	10Cb1	1885–1927	415.60	7.5YR 8/3	SI	MA	EH	–	7.82	1.37
	10Cb2	1927–1948	423.00	7.5YR 8/3	SI	MA	EH	–	7.77	1.37
	10Cb3	1948–1985	434.40	7.5YR 8/3	SI	MA	EH	–	7.78	1.37

The age data is cited from Chen et al. (2009). "–" means not detected.
[a] Descriptions and abbreviations follow the criteria described in the 'Field Book for Describing and Sampling Soils, version 3.0' (Schoeneberger et al., 2012 and Harden, 1982; Harden and Taylor, 1983).
[b] BD represents the bulk density.

Table 2
Representative chemical weathering indices.

Index (formula)[a]	Reference
Na_2O/Al_2O_3	Gu et al. (1999)
K_2O/Al_2O_3	Garrels and Mackenzie (1971)
$CIA = [Al_2O_3/(Al_2O_3 + CaO^* + Na_2O + K_2O)] \times 100$	Liu et al. (1995); Nesbitt and Young (1982)
$LWI = (CaO + Na_2O + MgO)/TiO_2$	Yang et al. (2006)
$PIA = (Al_2O_3\text{-}K_2O) \times 100/(Al_2O_3 + CaO^* + Na_2O\text{-}K_2O)$	Fedo et al. (1995)
$WIP = 100[(2Na_2O/0.35) + (MgO/0.9) + (2K_2O/0.25) + (CaO^*/0.7)]$	Parker (1970)
$CIW = Al_2O_3 \times 100/(Al_2O_3 + CaO^* + Na_2O)$	Harnois (1988)
Na_2O/K_2O	Li et al. (2007)
$CPA = [Al_2O_3/(Al_2O_3 + Na_2O)] \times 100$	Buggle et al. (2011)

[a] Molecular proportions of oxides. CaO* represents CaO proportion derived from silicate-bearing minerals only.

paleosol sequence. This is because grain size differences have few effects on it (Yang et al., 2006).

The Na_2O/K_2O (molar ratio) can be a proxy to measure the weathering intensity of plagioclase (Li et al., 2007). The Na is rich in plagioclase, and K is rich in feldspar. The weathering rate of plagioclase is much faster than K-feldspar. Hence the ratio of Na_2O/K_2O negatively correlates with the soil weathering intensity.

The CPA index is a suitable weathering index for indicating plagioclase weathering intensity. This index excludes the CaO* in calculation which can avoid the CaO* associated uncertainties due to the possible presence of secondary carbonates (Buggle et al., 2011).

2.4. Quantificational reconstruction analysis

L5 (423–403 ka BP) in the Chaoyang section and the uniform loess material (170–182 ka BP) of the Lingtai section with the least weathering intensity and uniform elemental distribution were selected as the un-weathered reference to compare weathering intensity in terms of losses and gains. TiO_2 was selected as the stable element to calculate the gain-loss factor using formula (1), revised from Garrels and Mackenzie (1971).

$$w = \frac{TiO_{2(reference)}}{TiO_{2(loess\text{-}or\text{-}paleosol)}} \quad (1)$$

Formula (2) was used to calculate the gain or loss for each oxide (%) based on the selected reference.

$$r(\%) = \left[\frac{(w \times Oxide_{(loess\text{-}or\text{-}paleosol)} - Oxide_{(reference)})}{Oxide_{(reference)}}\right] \times 100 \quad (2)$$

3. Results

3.1. Major elemental compositions on a volatile basis

Major elemental compositions on a volatile basis are presented in Fig. 2. This figure shows relatively great variability in loss on ignition

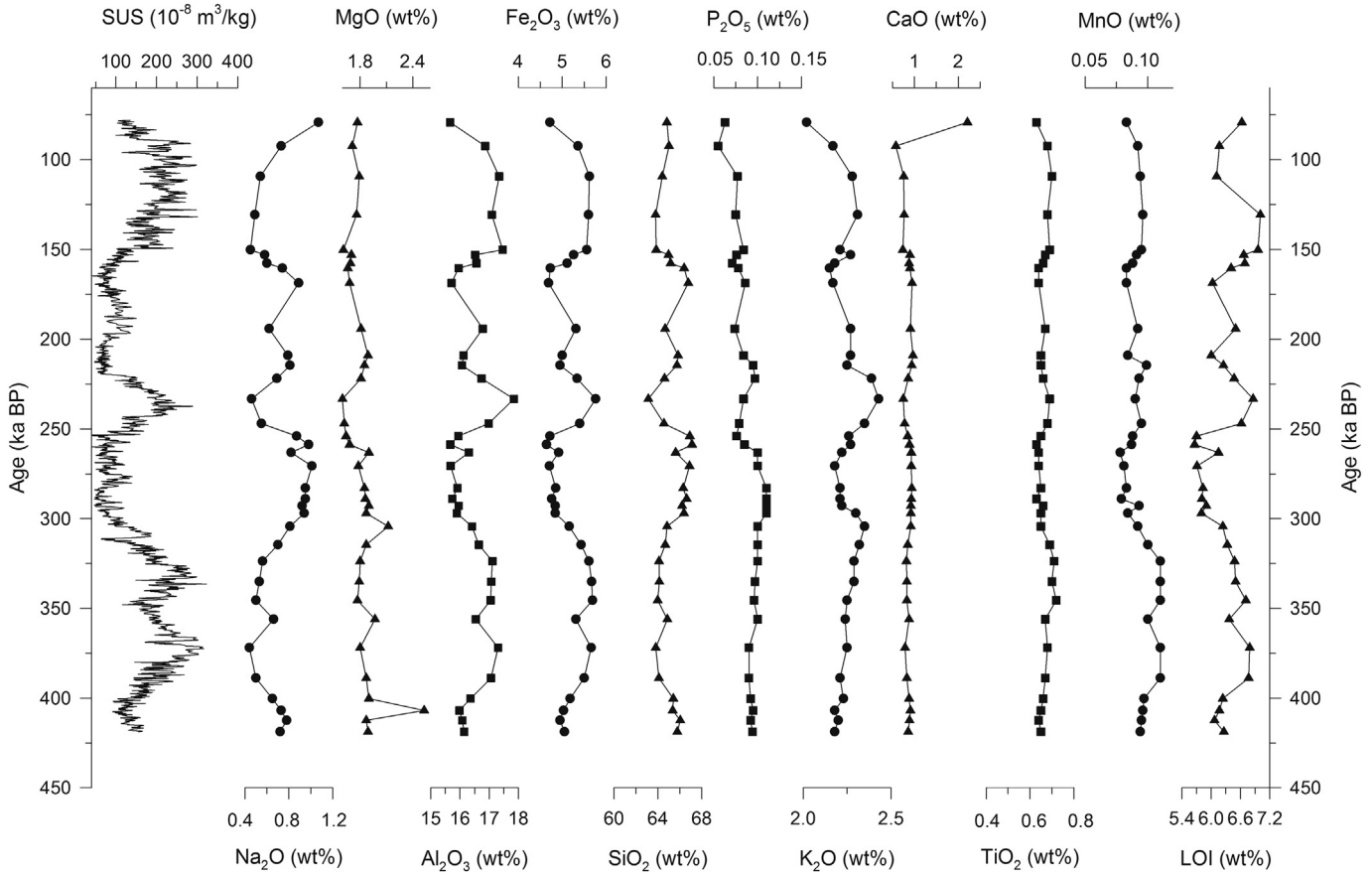

Fig. 2. Major elemental compositions (wt%) of loess and paleosol samples in the LOP of Chaoyang section, together with the magnetic susceptibility (SUS) records. LOI = the original loss on ignition.

(LOI) and major elemental concentrations through the LOP except for TiO_2, both for the loess and paleosols (Fig. 2). The relatively high and variable volatile phase may be responsible for the great variability in major elemental concentrations. LOI, as an indicator of the volatile phase, can reflect variances in hydrous phases (mainly clay minerals), carbonate content and organic matter (Ding et al., 2001; Gallet et al., 1996). Given the small amount of soil organic matter in loess (0.05%) and paleosols (0.06%) in this study, carbonates and hydrous phases may play a more important role in the LOI budget of loess and paleosol samples. LOI as measured for loess ranged from 5.66 to 6.62% with an average of 6.06% which was significantly less than for paleosols with a range of 6.11–7.01% and an average of 6.58% (Fig. 2). Carbonate contents were greater in the loess than in paleosols according to Sun et al. (2016). This suggests that the hydrous phase contributes more to the LOI budget of paleosols whereas carbonates contribute more to the LOI budget of loess. As soil magnetic susceptibility (SUS) enhancement can be commonly interpreted as a pedogenic proxy (Buggle et al., 2009; Heller and Tungsheng, 1984), paleosols can usually be distinguished from loess by greater values of SUS and concentrations of Fe_2O_3, Al_2O_3, LOI, K_2O and TiO_2 (Fig. 2). The average LOI (6.31%) of LOP in the Chaoyang section is significantly greater than for the Lingtai one (3.98%).

3.2. Recalculated major elemental compositions on a volatile-free basis

3.2.1. Elemental abundances

The studied LOP is weak alkaline material (average pH = 7.75), with no carbonate reaction to HCl (Table 1). The recalculated major elemental compositions on a volatile-free basis are depicted in Fig. 3. The major elemental abundances show relative spatial homogeneity with small values of the coefficient of variance (CV) < 15% (Essington, 2004), suggesting a relatively stable source to supply the LOP deposition. SiO_2, Al_2O_3 and Fe_2O_3 are dominant in the Chaoyang section. The trend in Al_2O_3 changes are consistent with those of Fe_2O_3, which is opposite to SiO_2 variances. Greater amounts of Fe_2O_3 and Al_2O_3 and lower concentrations of SiO_2 were determined for each paleosol layer when compared to adjacent loess. Paleosols have a greater average content of Al_2O_3 (18.15% vs. 17.16%) and Fe_2O_3 (5.83% vs. 5.26%) and a significantly lesser content of SiO_2 (69.17% vs. 70.47%) when compared to loess. These data suggest that paleosols have undergone a more intense pedogenic process of silification and ferrallitization than loess. The MnO content was 0.1% in average and was significantly greater in the paleosols (0.11%) than loess (0.09%). The K_2O concentration was significantly greater in paleosols (2.41% average) than in loess (2.39%). This may be attributed to K^+ being released from feldspar by weathering during a hot-wet climate of paleosol formation.

The relatively constant distribution of CaO (Mean = 0.92%, coefficient of variation (CV) = 9.01%), except for illuviated CaO from overlying horizons at a depth of 264 cm, and of TiO_2 (Mean = 0.71%, CV = 3.82%) contents with depth, indicates LOP was deposited from a relatively uniform material. The stable constituent TiO_2 was selected to calculate gains and losses (see Section 2) and reconstruct the soil formation. The TiO_2 stability in loess and paleosol samples can be explained by TiO_2 having extremely low solubility in water, uniformly distributes throughout the parent material and concentrates in weathering resistant minerals and non-clay fractions (Brewer, 1976; Egli et al., 2003; Smeck and Wilding, 1980).

The loess can be distinguished from paleosols by greater contents of Na_2O, MgO and SiO_2. The Na_2O and MgO distribution with depth negatively correlates with the Fe_2O_3 and Al_2O_3 one. The Na_2O content changes from 0.47% to 1.15% with an average of 0.77%. Loess has 0.89% Na_2O on average which is significantly greater than paleosols

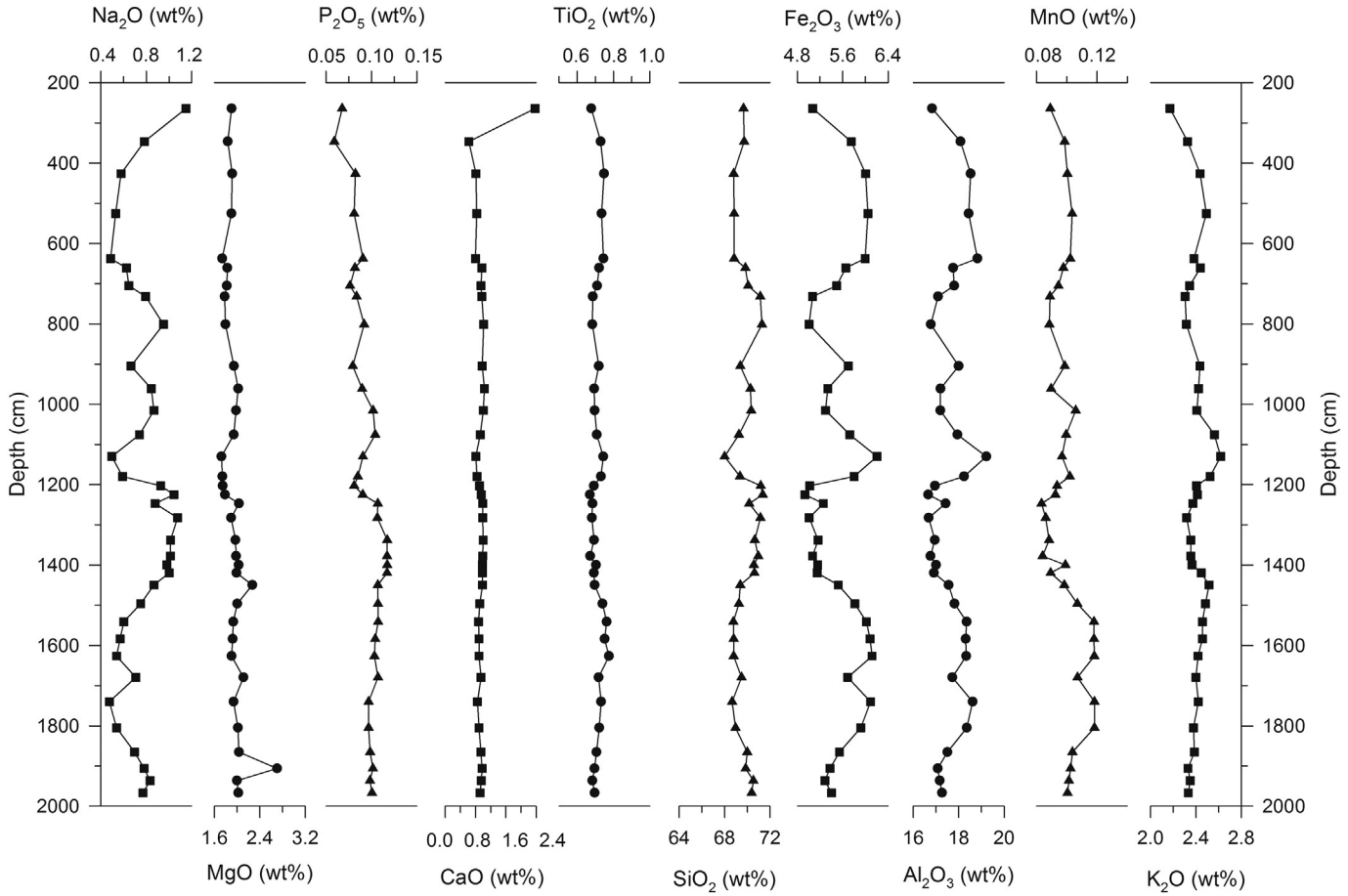

Fig. 3. The distribution of major elements (wt%) of loess and paleosol samples with depth (cm) in the LOP of Chaoyang section recalculated on a volatile-free basis.

(0.64%) indicating intense leaching of Na_2O in paleosols. This together with a high CV for Na_2O across the LOP indicate that Na_2O is mobile in loess. Furthermore, these elemental changes may provide information on climate change and loess deposition.

The close agreement between the paleosols and loess for most of the major elements is apparent in Fig. 4. The marked correlation of major elemental concentrations between the paleosol and loess supports the view that the paleosols share the same source with the loess. The main processes of silification and ferrallitization, along with the relative leaching of Si and mobile elements including Ca, K, and Na, and residual enrichment of less mobile elements such as Fe, Al and Ti, occurred in the Chaoyang section during 423–77 ka BP.

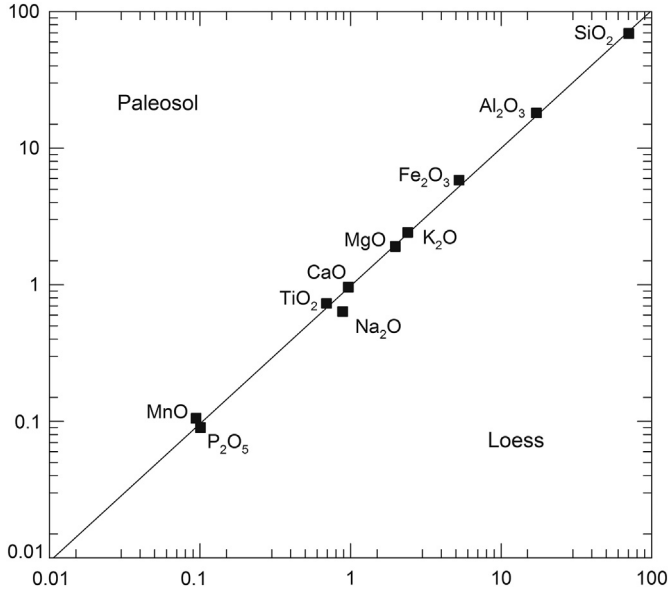

Fig. 4. The comparison diagram of major elemental compositions between paleosol and loess samples in the LOP of Chaoyang section.

3.2.2. *Chaoyang section compared to Lingtai section*

The AUCC-normalized major elemental distributions in the Chaoyang loess-paleosol are generally comparable and very similar to those in the Lingtai loess-paleosol (Fig. 5A). The good agreement and high correlation of the major elemental compositions between loess-paleosol samples in the Chaoyang and Lingtai sections (Fig. 5B) indicates that both the Lingtai (Ding et al., 1999) and Chaoyang sections (Sun et al., 2016) are wind-blown in origin and may originate predominantly from a similar source (Fig. 5). Nevertheless, there are differences in absolute enrichment relative to the AUCC and there are some minor deviations in the patterns. The geochemical composition of the Chaoyang and Lingtai sections primarily indicates depletions with respect to AUCC except for Al, Si, Ti, Mn and Fe (Fig. 5A). The depletion of Ca, Na and P is notable as indicated in Fig. 5A. This deviation from the AUCC may reflect one of the weathering characteristics of the continent. The amount of Al and Fe enrichment and Ca, P and Na depletion with respect to the AUCC are greater in the Chaoyang section than in the Lingtai section.

In general, a similar trend in elemental distribution with time between Lingtai and Chaoyang sections can be observed in Fig. 6. Larger fluctuations in amplitudes of the elemental variability were found in the Chaoyang section when compared to the Lingtai one. A larger fluctuation was found for the Lingtai section at around 412 ka BP compared

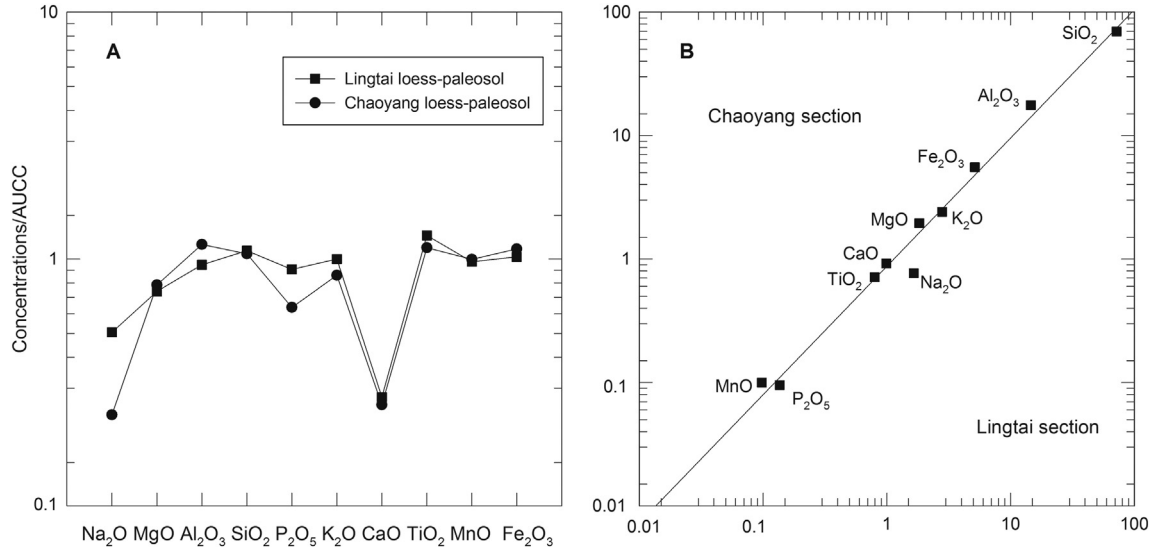

Fig. 5. (A) AUCC-normalized pattern of major elemental distributions of loess and paleosol samples in the LOP of Chaoyang section and Lingtai section. These data was recalculated on a volatile-free basis. (B) The comparison diagram of major elemental compositions between Chaoyang and Lingtai sections. The major elemental data of Lingtai section was cited from Yang et al. (2006). AUCC (the average upper continental crust) was cited from Rudnick and Gao (2003).

to the Chaoyang one. From 423 ka BP to 77 ka BP, a general increasing trend in Na_2O, SiO_2 and CaO, and a decreasing trend in Al_2O_3, Fe_2O_3 and P_2O_5 occurred in both the Chaoyang and Lingtai sections (Fig. 6). A nearly constant trend in TiO_2 and MnO was found in the Chaoyang and Lingtai sections. A slight decrease in MgO and K_2O in the Chaoyang section was also found, while a slight increase was found for the Lingtai section. These trends indicate a decreasing intensity of pedogenesis from 423 ka BP to 77 ka BP.

The Lingtai section compared to the Chaoyang section has smaller amounts of Na_2O (0.77% vs. 1.65% average), SiO_2 (69.84% vs. 71.96%), P_2O_5 (0.10% vs. 0.14%), K_2O (2.40% vs. 2.80%), CaO (0.92% vs. 0.99%), TiO_2 (0.71% vs. 0.80%), and equal amounts of MnO (0.10%), and greater amounts of MgO (1.95% vs. 1.83%), Al_2O_3 (17.64% vs. 14.60%), Fe_2O_3 (5.54% vs. 5.14%) (Fig. 6) and LOI (6.31% vs. 3.98%), respectively (Fig. 2). These data support the view that the Chaoyang section has undergone a more intense pedogenesis of silification and ferrallitization than the Lingtai one. In contrast, the Lingtai section may have had a greater deposition rate than the Chaoyang section given the greater Na_2O content in the Lingtai section. Paleosols can be characterized by greater amounts of Fe_2O_3 and Al_2O_3, and lesser amounts of Na_2O, CaO and SiO_2 in both sections. This suggests that both the Chaoyang and Lingtai sections illustrate a record of past climates; however, the Chaoyang section demonstrates greater pedogenesis which may indicate a more intense weathering environment.

4. Discussion

4.1. Characteristics of elemental ratios and chemical weathering intensity

4.1.1. Elemental ratios

Variance in grain size has been reported to have an influence on the chemical composition of loess and paleosols (Ding et al., 2001). Pedogenic processes following silt deposition (Sun et al., 2016) may complicate the interpretation of chemical weathering by different physical properties such as grain size between the loess and paleosols. The uniform texture of silt and clay-free grain size distribution in the Chaoyang section have been reported by Sun et al. (2016). Therefore, chemical weathering indices may assist reconstruction of weathering history.

Variances in chemical indices at Chaoyang together with the bulk magnetic susceptibility (SUS) record are given in Fig. 7. The CPA, CIA, CIW and PIA trends are mostly consistent with the SUS trend, while they are significantly opposite to LWI, WIP, Kr, Na_2O/Al_2O_3 and K_2O/Al_2O_3. A lesser amplitude of change is apparent in LWI and K_2O/Al_2O_3 when compared to the other indices. This may indicate that LWI and K_2O/Al_2O_3 are less sensitive to loess pedogenic environmental changes than other indices. A similar trend of more intense weathering was observed in the older paleosol S3 (maximum) during 225–243 ka BP. The peak values generally decreased from 403 to 243 ka BP and from 243 to 77 ka BP which indicates that the intensity of feldspar weathering was decreasing. The feldspar weathering intensity in the L5 (423–403 ka BP) is comparable to L4 (311–243 ka BP) and less than for S4 (403–311 ka BP). The detailed patterns of CPA, CIA, CIW and PIA associated with feldspar weathering resemble each other closely, and suggest different pedogenic phases. The greater values of CPA, CIA, CIW and PIA corresponding to smaller values of LWI (Yang et al., 2006), WIP, Kr, Na_2O/Al_2O_3 and K_2O/Al_2O_3 are interpreted as being associated with stronger pedogenic weathering (Duzgoren-Aydin et al., 2002). This supports the view that well developed paleosols have greater SUS values as peaks in Fig. 7 with greater chemical weathering. The greater weathering indices such as CPA, CIA, CIW and PIA reflect stronger pedogenic weathering intensity (Duzgoren-Aydin et al., 2002), lesser loess accumulation (e.g. An et al., 1991; Guo et al., 2000; Liu, 1985; Sun et al., 2016, 2016), and smaller ratio between loess accumulation and weathering intensity in more humid environments (Sun et al., 2016, 2016). Greater weathering indices of LWI (Yang et al., 2006), WIP, Kr, Na_2O/Al_2O_3 and K_2O/Al_2O_3 reflect weaker pedogenic weathering intensity, greater loess accumulation (e.g. An et al., 1991; Guo et al., 2000; Liu, 1985; Sun et al., 2016, 2016), and larger ratio between loess accumulation and weathering intensity in dryer environments (Sun et al., 2016, 2016) rather that more humid environments. Based on the variability in these chemical weathering indices corresponding to SUS and field observations (Sun et al., 2016), the formation period of the Chaoyang section can be separated into eight sub-periods including four with greater chemical weathering intensity (e.g. 159–77 ka BP, 208–176 ka BP, 243–225 ka BP and 403–311 ka BP) and four characterized by lesser chemical weathering intensity (e.g. 176–159 ka BP, 225–208 ka BP, 311–243 ka BP and 423–403 ka BP). From 109 to 130 ka BP, an increasing trend in K_2O/Al_2O_3 is different from other weathering indices which may be caused by K^+ released from intensely weathered feldspar or attributed to a relatively high concentration of illite-mica (Sun et al., 2016) under a wet-hot climate. Soluble and mobile elements of K and Na are easily removed by chemical weathering (Duzgoren-Aydin et al., 2002; Loughnan, 1969). In

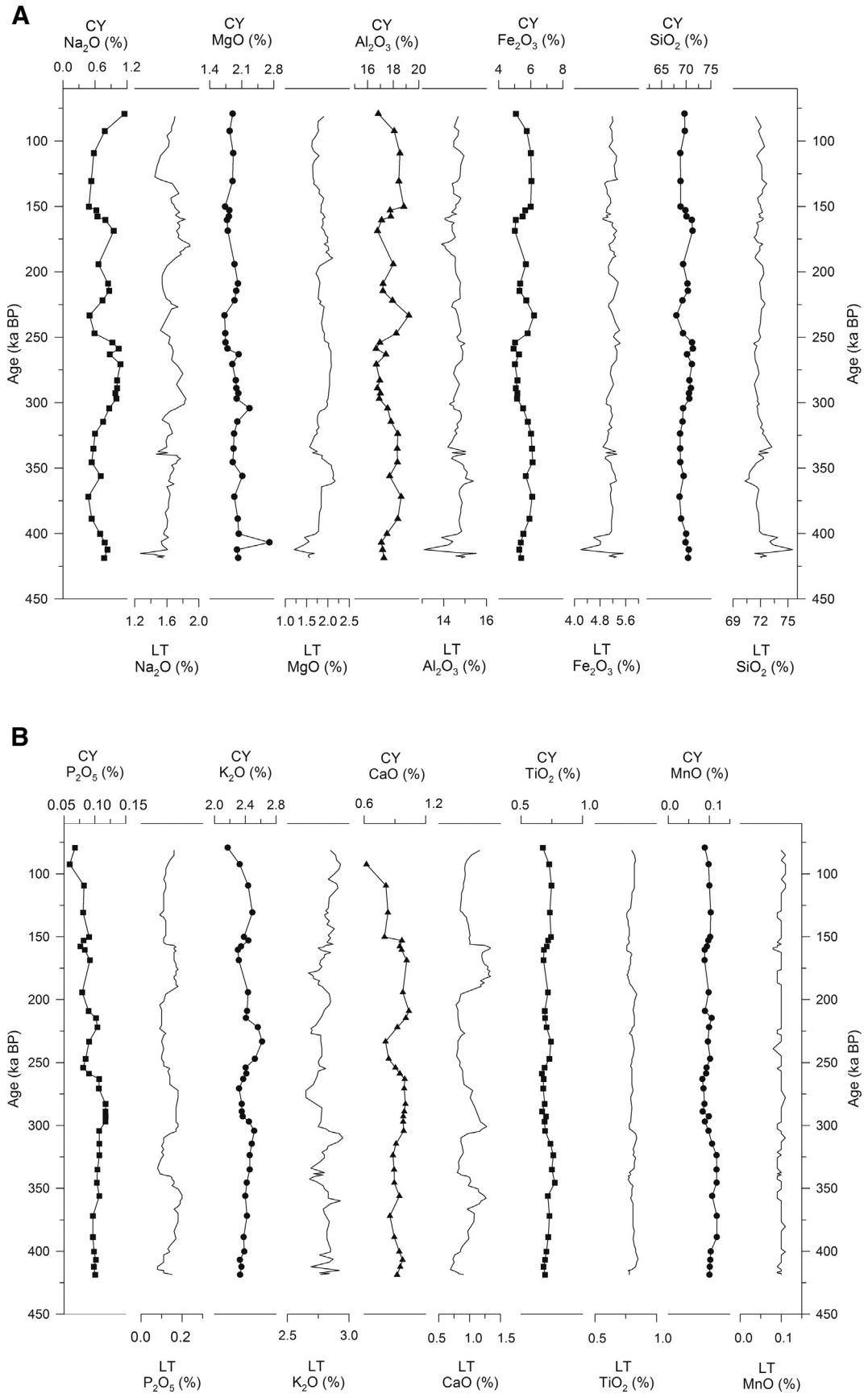

Fig. 6. A. Major elemental compositions (wt%) of loess and paleosol samples in the LOP of Chaoyang section (CY) and Lingtai section (LT). These data were recalculated on a volatile-free basis. The major elemental data of Lingtai section was cited from Yang et al. (2006). B. Major elemental compositions (wt%) of loess and paleosol samples in the LOP of Chaoyang section (CY) and Lingtai section (LT). These data were recalculated on a volatile-free basis. The major elemental data of Lingtai section was cited from Yang et al. (2006).

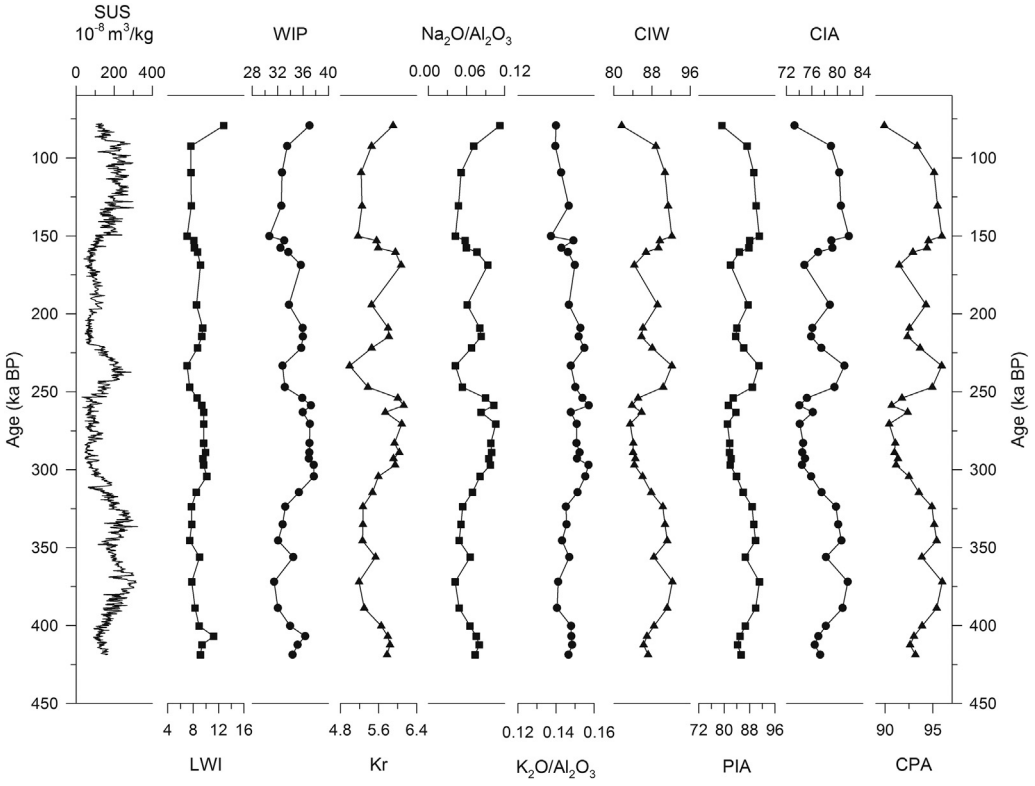

Fig. 7. Variances of chemical weathering indices including CPA, LWI, CIA, PIA, WIP, PIW, Kr, K_2O/Al_2O_3 and Na_2O/Al_2O_3 (see Section 2.3) in the Chaoyang section, together with the magnetic susceptibility (SUS) records. These indices were calculated on a volatile-free basis.

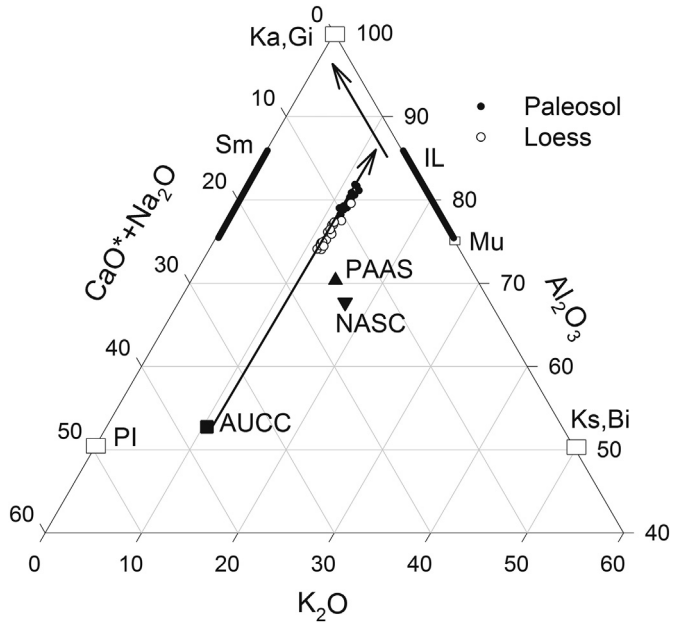

Fig. 8. Chemical weathering trends of A-CN-K in the Chaoyang section. Note that only the upper part of the ternary diagram is presented, which is of the interest for this study. The AUCC values were cited from Rudnick and Gao (2003). These data was recalculated on a volatile-free basis. Two widely quoted post-Archean shale averages of PAAS (post-Archean Australian shale) and NASC (North American shale composite) were cited from Condie (1993) for comparison with Chaoyang section. The CaO* denotes the CaO in silicate minerals only. The arrows are drawn to reflect the plotted data only. The open squares denote idealized mineral compositions used for orientation purposes according to Nesbitt and Young (1982) and McLennan (1993). Ka = Kaolinite; Gi = Gibbsite; IL = Illite; Mu = Muscovite; Ks = Potash Feldspar; Bi = Biotite; Sm = Smectite; PI = Plagioclase.

comparison with the AUCC (Rudnick and Gao, 2003), significant depletions of Na and K were found for both the loess and paleosols according to the comparison diagram of K_2O/Al_2O_3 vs. Na_2O_3/Al_2O_3 in Fig. 8. More Na depletion (release) than K depletion is illustrated in Fig. 8. This is because K phases (prominent K-feldspar) in loess-paleosol sequences have a stronger weathering resistance than Na phases (prominent plagioclase) (Nesbitt and Young, 1984; Nesbitt and Young, 1989). In addition, larger amounts of K may also be fixed on clay minerals than Na due to a larger ionic radius than Na facilitating absorption to clay minerals. Furthermore, the paleosol has a larger Na depletion ($Na_2O_3/Al_2O_3 = 0.06$ average) than the loess ($Na_2O_3/Al_2O_3 = 0.09$).

The LWI is a reliable proxy because it is subject to little grain-size influence (Yang et al., 2006). The LWI is greater for loess than for paleosols (Fig. 7). Lesser values of LWI consistently correspond to greater SUS values. The high carbonate content in the loess contributes to the higher LWI values when compared to paleosols. Greater CIA values were found in four paleosols (79.43 in average) reflecting the dominance of warm-humid weathering conditions whereas the loess (75.86) had lower CIA values. Within each paleosol the greatest weathering intensity was in the middle and/or lower part of each profile which indicates the most intense weathering period (Fig. 7). The average CIA value of S1–2 (79.04), L2 (75.91), S2 (78.84), L3 (77.08), L4 (75.35), S4 (79.64) and L5 (76.93) are classified as intermediate weathering according to Fedo et al. (1995), and of S3 for 81.13 as extreme weathering. Hence S3 is determined to be the most developed horizon corresponding well to the reddest color, strongest structure and most intense desilication and fersiallitization with the lowest Kr value (4.99 in average) and the greatest Fe_2O_3 and Al_2O_3 accumulation. S3 also has the most abundance of illite which may have been derived from the weathering of K-feldspar in situ. L4 has the lowest weathering intensity with weak pedogenic characteristics including pale color, poor structure, and relative uniform elemental distributions. This weathering intensity trend in the Chaoyang section also corresponds well to the trend

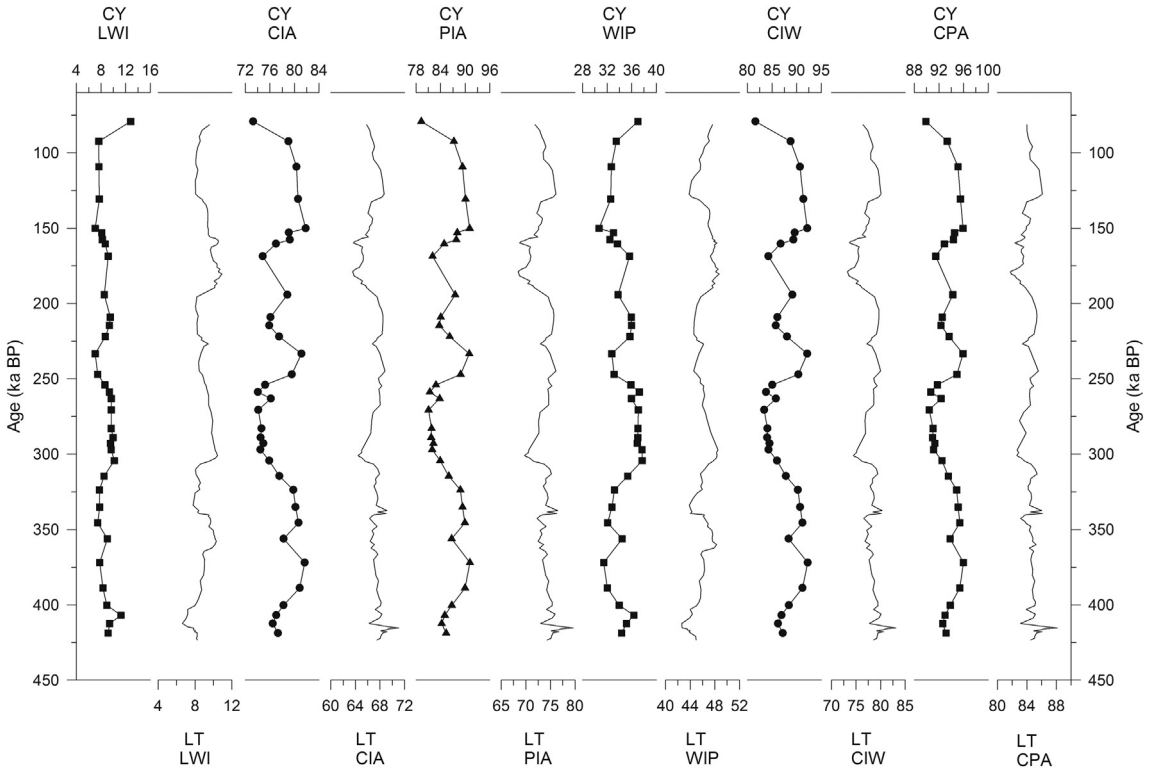

Fig. 9. Variances of chemical weathering indices including LWI, CIA, PIA, WIP and PIW (see Section 2.3) in the Chaoyang section (CY) and Lingtai section (LT). These indices were recalculated on a volatile-free basis. The major elemental data of the Lingtai section was cited from Yang et al. (2006).

shown by other chemical weathering indicators (Fig. 7). There is a significant relationship between CIA and LWI (correlation coefficient $R = -0.813$), CIA and PIA ($R = 0.997$), CIA and WIP ($R = -0.946$), CIA and CIW ($R = 0.995$), CIA and Kr ($R = -0.935$), CIA and Na_2O/Al_2O_3 ($R = -0.988$), CIA and CPA ($R = 0.989$), CIA and K_2O/Al_2O_3 ($R = -0.636$), and CIA and Na_2O/K_2O ($R = -0.969$).

4.1.2. Chemical weathering trends

The ternary diagram of Al_2O_3-(CaO* + Na_2O)-K_2O of the Chaoyang section was plotted primarily on a plagioclase weathering line, in the same direction of NASC and PAAS (Condie, 1993) and originating from AUCC (Rudnick and Gao, 2003) (Fig. 8). CIA values range from 52.74 for AUCC (virtually no weathering), to 81.13 on average for S3 (intense weathering). The data in Fig. 8 also supports the view that the loess has been weakly weathered to different extents than the paleosols which should not be assumed as the initial composition for the paleosols. Feldspar weathering is predominant in the chemical weathering of the upper crustal rocks. The Al_2O_3-(CaO* + Na_2O)-K_2O system is proposed to illustrate much of the chemical variation resulting from weathering (Nesbitt and Young, 1984; Nesbitt and Young, 1989). The weathering process can be understood as an acid-base reaction. The acid (usually H_2CO_3) can be neutralized by a solid base (the feldspar or glass) with production of secondary clay minerals and dissolved salts (Garrels and Mackenzie, 1967; Helgeson et al., 1969). The weathering of feldspars usually produces illite and kaolinite (Fig. 8), and the mafic minerals and glass commonly weather to smectite, illite and kaolinite. The CIA for the un-weathered feldspar is 50, for the illite and smectite ranges from 75 to 85, and for the kaolinite is 100 (Nesbitt and Young, 1982). Based on these, the weathering trend illustrated by the two arrows in Fig. 8 indicates this trend. The paleosol and loess samples of the Chaoyang section are in a parallel line to the A-CN join (see the arrow at the bottom of Fig. 8). The uniformity of the parent material of the loess-paleosol can be evaluated using variations in the K-feldspar/plagioclase ratio as revealed by the A-CN-K ternary diagram in terms of a scatter of data-points parallel to CN-K (Buggle et al., 2011). A narrow weathering line of the Chaoyang loess-paleosol indicates that the aluminosilicate composition of parent material in the Chaoyang section was relatively uniform according to Buggle et al. (2011). This is a typical distribution for the loess-paleosol sequence with different chemical weathering intensities (Buggle et al., 2008). The plagioclase in the loess and paleosols first weathered which allowed soluble elements of Ca and Na to be removed. The depletion rate of Ca and Na is greater in paleosols than in the loess (Fig. 8). This indicates that the paleosols in the Chaoyang section have undergone more intense weathering process compared to the loess. The plagioclase in the paleosols has been intensely weathered, with a larger extent of Ca and Na removed compared to the loess. The paleosol samples were closer to the Al_2O_3 apex than the loess (Fig. 8), which indicates the particle size of paleosol is finer than the loess due to abundant alumino-silicate clay minerals in paleosols derived from the intense pedogenesis (Nesbitt et al., 1996). The paleosol data at the fore end of the long arrow (closed dots including S3) slightly deviates to parallel the A-K line and points to the Al_2O_3-apex. This may indicate weathering of potassic phases including K-feldspar, illite or mica with little K release (Nesbitt and Young, 1984; Nesbitt and Young, 1989). The molar ratio of Na_2O/K_2O reflects weathering intensity (Li et al., 2007). S3 has the smallest Na_2O/K_2O value (0.29) indicating intense weathering in a weathering stage of slight K removal from K-feldspar during 225–243 ka BP. This is consistent with an increasing K_2O content during 225–243 ka BP (Fig. 3). Although the weathering intensity of S3 (CIA = 81.13) can be classified as extreme according to Fedo et al. (1995), illite is the predominant clay mineral in S3 which has not been weathered to the kaolinite stage. L4 with the greatest Na_2O/K_2O (0.59) is at the end of the long arrow (open dots) which suggests that the weathering intensity of L4 was slight and the climate was cold-dry during 243–311 ka BP.

4.1.3. The Chaoyang section compared to the Lingtai one

The weathering index curves for the Lingtai section are much smoother due to a greater sampling resolution than for the Chaoyang section (Fig. 9). A similar trend in weathering intensity is evident in the

Table 3
Statistical variation coefficients of selected chemical weathering indices in the Chaoyang and Lingtai sections.

Section	LWI			CIA			PIA			WIP			CPA		
	Mean	SD[b]	CV[c]	Mean	SD	CV	Mean	SD	CV	Mean	SD	CV	Mean	SD	CV
Chaoyang	8.82	1.19	13.53	77.60	2.50	3.22	85.83	3.35	3.91	34.63	1.99	5.75	93.31	1.77	1.90
Lingtai	9.03	0.94	10.43	65.93	1.55	2.35	71.97	2.28	3.17	46.63	1.57	3.36	84.33	1.03	1.22
AUCC[a]	22.32	–	–	52.74	–	–	53.47	–	–	68.39	–	–	74.11	–	–

[a] AUCC = the Average Upper Continental Crust (Rudnick and Gao, 2003).
[b] SD = Standard deviation.
[c] CV = Coefficient of variation (%).

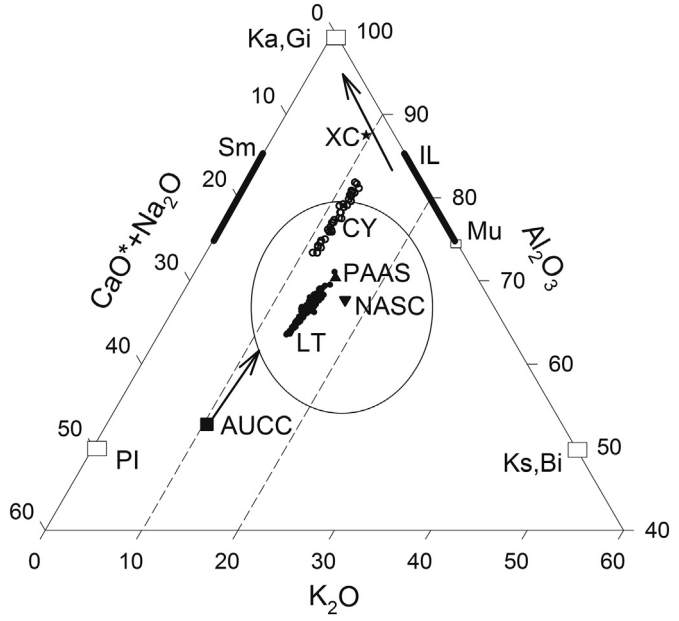

Fig. 10. Chemical weathering trends of A-CN-K in the Chaoyang (CY) and Lingtai (LT) sections. Note that only the upper part of the ternary diagram is presented, which is of the interest for this study. The AUCC values were cited from Rudnick and Gao (2003). The data of Xuancheng eolian red clay (XC) was cited from Li et al. (2007). These data was recalculated on a volatile-free basis. Two widely quoted post-Archean shale averages of PAAS (post-Archean Australian shale) and NASC (North American shale composite) were cited from Condie (1993) for comparison. The CaO* denotes the CaO in silicate minerals only. The arrows were drawn to reflect the plotted data only. The open squares denote idealized mineral compositions according to McLennan (1993); Nesbitt and Young (1982). Ka = Kaolinite; Gi = Gibbsite; IL = Illite; Mu = Muscovite; Ks = Potash Feldspar; Bi = Biotite; Sm = Smectite; PI = Plagioclase.

Chaoyang and Lingtai sections. An opposite trend during 225–208 ka BP occurred between the Chaoyang and Lingtai sections. This may have been caused by a regional climate change which is different between the Chaoyang and Lingtai sections during 225–208 ka BP. In general, CIA, CPA, PIA and CIW decrease gradually, while LWI and WIP increase from 423 ka BP to 77 ka BP. Chemical weathering indices were calculated for AUCC, such as LWI (22.32), CIA (52.74), PIA (53.47), CPA (74.11), WIP (68.39) and CIW (58.87) for comparison. Compared to AUCC, the Chaoyang and Lingtai sections have significantly greater chemical weathering index values of CPA, CIA, PIA and CIW and smaller values of LWI and WIP (Table 3). This indicates that the Chaoyang and Lingtai sections have experienced relatively more intense weathering than the AUCC. A larger amplitude in variability of these indices (Fig. 9) with a greater coefficient of variation values (Table 3) was observed in the Chaoyang section compared to the Lingtai one. This may indicate that larger-amplitude climate changes have been recorded in the Chaoyang section than in the Lingtai one. The chemical weathering intensity is much greater in the Chaoyang section than the Lingtai one (Fig. 9 and Table 3). Greater Na_2O and P_2O_5 in the Lingtai section than in the Chaoyang one (Fig. 5A) support this conclusion.

The alternation of loess and paleosols in the Chaoyang and Lingtai sections has been revealed through these chemical weathering indices as shown in Fig. 9. Paleosols have greater CPA, CIA, PIA and CIW values and lower LWI and WIP ones compared to the adjacent loess (Fig. 9).

The data of Chaoyang and Lingtai sections is distributed along with AUCC to PAAS and NASC in Fig. 10. This suggests that the weathering of the Chaoyang and Lingtai sections is consistent with the terrestrial weathering trend. The weathering intensity of the Chaoyang section is significantly greater than of the Lingtai one. The data inside the big open circle (BOC) can indicate intermediate weathering intensity according to Fedo et al. (1995). The data line of the Chaoyang section is parallel to the data line of the Lingtai section, and the A-CN line. This supports the view that the Chaoyang and Lingtai sections are comparable. The compositions of parent material in both the Chaoyang and Lingtai sections are uniform which indicates that they are appropriate research materials on chemical weathering history under different climatic changes. The main process is weathering of plagioclase to illite. The weathering of plagioclase is obviously more intense in the Chaoyang section than in the Lingtai one, which also can be supported by the lower molar ratio of Na_2O/K_2O in the Chaoyang section for 0.49 (CV = 27%) compared to the Lingtai one for 0.89 (CV = 7.75%). The Chaoyang samples are closer to the Al_2O_3 apex than the Lingtai ones (Fig. 10) due to abundant aluminous clay minerals, which indicate that the particle size of the Chaoyang section is finer than the Lingtai one according to Nesbitt et al. (1996). The deposition of loess was synchronous with the pedogenic processes (Sun et al., 2016). Pedogenesis has more influence on the Chaoyang section while the loess deposition has more influence on the Lingtai one as inferred from the weathering intensity of plagioclase and its variations. The data line for the Chaoyang section is outside the BOC, and the Xuancheng data approach the A-K line to suggest extreme weathering according to Fedo et al. (1995). This line is within the weathering trend of illite to kaolinite. The Xuancheng red clay was previously in the predominant kaolinite stage whereas the Chaoyang section was mainly in illite stage. The values of Fe_2O_3/Al_2O_3 ratio are around 0.2 in both Chaoyang (0.20) and Lingtai sections (0.22) which are consistent with AUCC (0.21), NASC (0.21) and PAAS (0.22). This provides supporting evidence that the Chaoyang and Lingtai sections have a source similar to AUCC.

Although a similar source can be inferred, more evidence is still needed to ascertain the source provenance for Chaoyang and Lingtai sections. Do they have the same source or have a similar but different source? A geochemical approach could be used to help with identifying a potential source (Buggle et al., 2008). Elemental ratios such as Fe_2O_3/Al_2O_3, Fe_2O_3/TiO_2 and Al_2O_3/TiO_2 should be first used to estimate the effects of weathering and sorting. After evaluation of possible biasing effects, the sediment origin may be confirmed on the basis of similarities in elemental ratios between a potential source and the studied sediment. Different major potential source areas with distinctly different elemental compositions are an essential prerequisite of successful evaluation. Although major elemental data for the Chaoyang and Lingtai sections have already provided some insights into the potential source, information on other major potential source areas such as

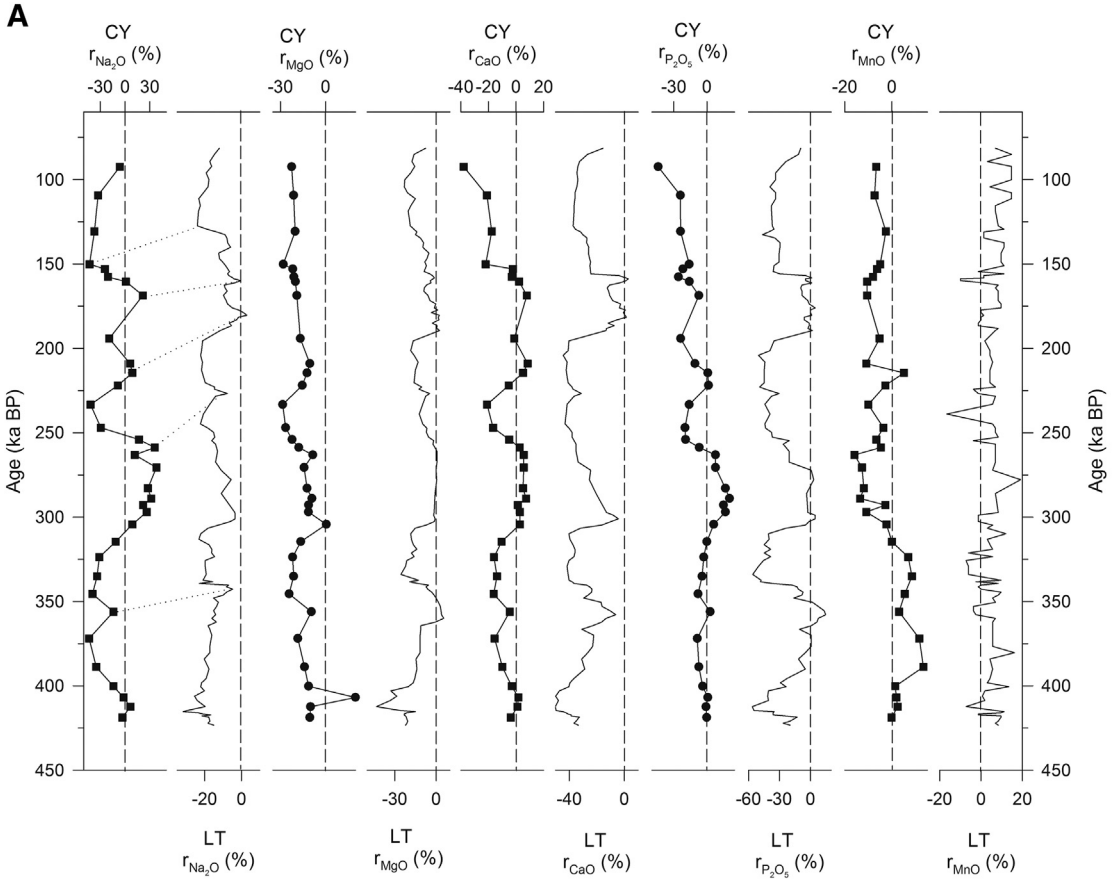

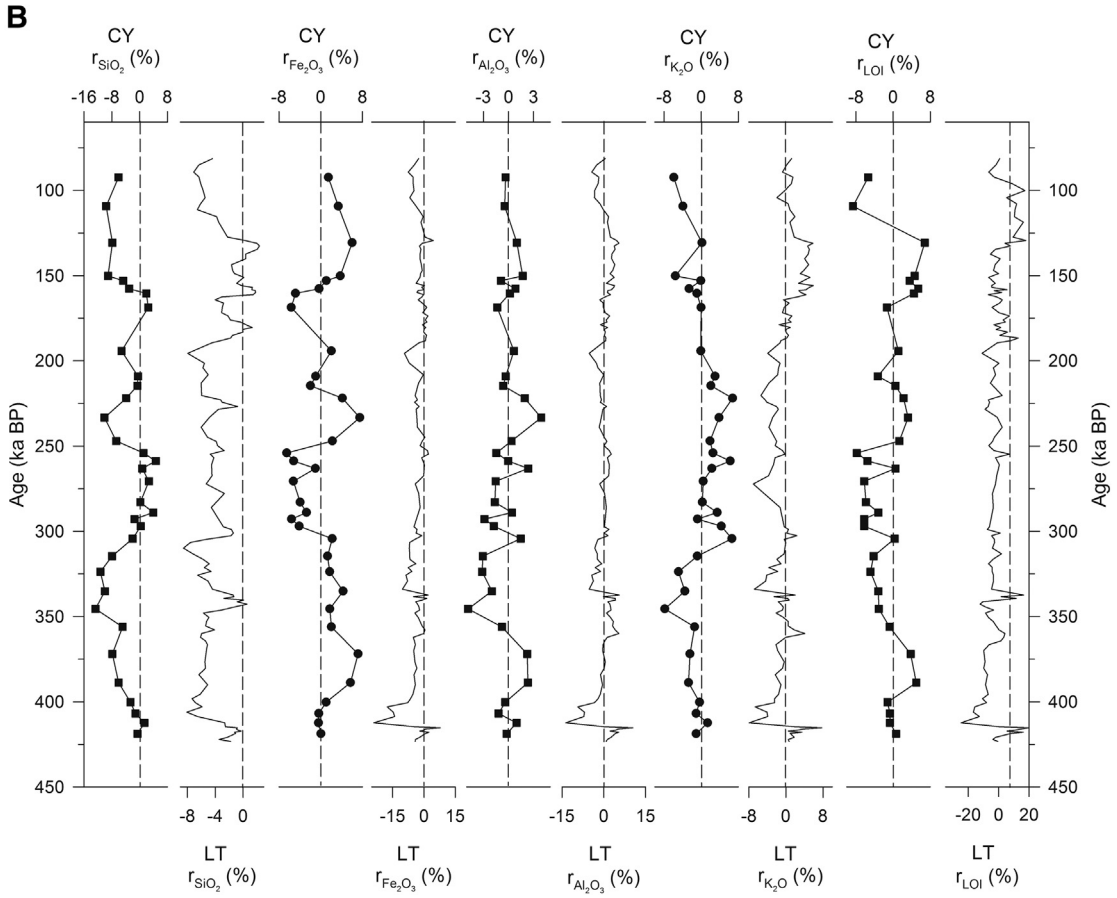

(caption on next page)

Fig. 11. A. Gains and losses (%) (see Section 2.4) of major elemental compositions and of the LOI with time for the Chaoyang section (CY) and Lingtai section (LT) based on the selected reference, respectively, using TiO_2 as a stable element for re-correction. All data was recalculated on a volatile-free basis. The major elemental data of Lingtai section was cited from Yang et al. (2006) and recalculated here. B. Gains and losses (%) (see Section 2.4) of major elemental compositions and of the LOI with time for the Chaoyang section (CY) and Lingtai section (LT) based on the selected reference, respectively, using TiO_2 as a stable element for reconstruction. All data was recalculated on a volatile-free basis. The major elemental data of the Lingtai section was cited from Yang et al. (2006) and recalculated.

Horqin and Qtindag deserts are still needed. More loess paleosol sequences like the Chaoyang one in northeastern China are necessary for establishing the relationship between source provenance of the Chaoyang and Lingtai sections. A detailed discussion relative to the loess provenance of the Chaoyang section is beyond the scope of this study and will be given elsewhere (in the next paper) together with information on potential sources.

4.2. Mass balance interpretations

Paleosols and loess have undergone different degrees of weathering as shown in Section 3.2. The loess buried at depth should be also considered as a weakly weathered paleosol and can be differentiated by the poorly developed features from the paleosol category (Sun et al., 2016). Therefore the loess underlying a paleosol supposed to be the initial composition of the paleosol was not appropriate. According to the principle of selecting a reference for loess deposition to reconstruct soil formation as proposed by Brewer (1976), the reference parent material was selected for the Chaoyang and Lingtai sections. L5 has been well defined for selection as the reference for the Chaoyang section based on field observations, geochemical features, micro-morphological features and particle size distribution characteristics (Sun et al., 2016). Although the micro-morphological features of the Lingtai section are not available, the uniform loess material (170–182 ka BP) of the Lingtai section with the least weathered intensity such as CIA and uniform elemental distribution was selected as the reference for reconstructing the loess-paleosol sequence. Then the gains and losses in the loess-paleosol in the Chaoyang and Lingtai sections were calculated by Eqs. (1) and (2) using TiO_2 as the constant element (Figs. 4 and 7).

Gains and losses of major elements and of LOI for the Chaoyang and Lingtai sections are presented in Fig. 11. In general, the distributions of losses and gains in the Chaoyang section are relatively consistent with those trends found in the Lingtai section (Fig. 11). For example, the consistent trend can be obviously observed in the rNa_2O (%) distribution in Fig. 11A. These indicate that both the Lingtai and Chaoyang sections record the global climatic signals. The amplitude of elemental gains and losses such as for SiO_2, Fe_2O_3 and Al_2O_3 is larger in the Chaoyang section than in the Lingtai one. The difference may be caused by the different regional weathering environments. Furthermore, eight sub-periods of different pedogenic environments under different climate intensities can be recognized, which are consistent with the conclusions in Section 3.2.1.

During 159–77 ka BP, 208–176 ka BP, 243–225 ka BP and 403–311 ka BP, a loss of SiO_2 and a gain of Fe_2O_3 and Al_2O_3 can be observed in Fig. 11B. The amounts of gain are lesser in the Lingtai section than in the Chaoyang one. The main process is feldspar weathering to predominantly illite (Section 4.1.3). The weathered paleosol in the Lingtai section (for example, development loess of 159–77 ka BP) has low losses of SiO_2 and gains of Fe_2O_3 and Al_2O_3, whereas large gains in K_2O were determined. This contradiction indicates that loess deposition has played a role in altering the loess and the $CaCO_3$ contributes more to the high LOI in the Lingtai section than the clay minerals. The greater losses of SiO_2 (3.54% on average) and gains of Fe_2O_3 (0.77%) and Al_2O_3 (0.33%) corresponding to gains of K_2O (0.41%), supports that relatively intense desilication and fersiallitization primarily occurred in the Chaoyang section. This suggests that clay minerals from pedogenesis contribute more to the large LOI in the Chaoyang section. The large losses of CaO (28.03% on average) and Na_2O (14.03%) in the Lingtai section (Fig. 11A) indicate that Ca and Na leaching were still predominant in the Lingtai section. The weathering intensity is more intense in the paleosol than loess (Fig. 11) in both the Chaoyang and Lingtai sections. Compared to the Xuancheng eolian red clay (predominantly kaolinite), the weathering intensity of the Chaoyang section was still at the intermediate weathering stage (mainly illite). Future research should be done to provide more insight into the relationship between the provenance sources of the Chaoyang and Lingtai sections which would be helpful for understanding the weathering history and reconstruction of the paleoclimates.

5. Conclusions

The investigated loess-paleosol sequence is in a poorly investigated region beyond the north-east corner of the Chinese Loess Plateau. It is comparable to that in the central Chinese Loess Plateau, and shares a similar source provenance. Major elemental distributions such as K, Na, Ca, Si, Fe, Al and their ratios including CPA, CIA and Na_2O/K_2O record the loess-paleosol weathering sequence. Comparison using linear regression of major elemental distributions and A-CN-K can help with estimating the uniformity of loess-paleosols. The weathering trend in the loess-paleosol sequence in northeast China is consistent with that in the central Chinese Loess Plateau, and the weathering intensity was greater than in the former. The gains and losses of different elements in the loess-paleosol sequences correspond to the weathering indices, elemental compositions and magnetic susceptibility, and can be used to separate the 77–423 ka BP into four sub-periods with greater chemical weathering (e.g. 159–77 ka BP, 208–176 ka BP, 243–225 ka BP and 403–311 ka BP) and four sub-periods characterized by relative lesser chemical weathering (e.g. 176–159 ka BP, 225–208 ka BP, 311–243 ka BP and 423–403 ka BP). A weathering sequence of AUCC < Lingtai section < Chaoyang section < Xuancheng section is proposed to assist with understanding the weathering history of the widely distributed Chinese loess.

Acknowledgements

The authors sincerely thank Professor Alfred E. Hartemink, University of Wisconsin-Madison, USA and Professor Donald Davidson, University of Stirling, UK, for reviewing an earlier version of the paper; and all the students and staff who provided their input to this study. Also thanks go to the National Natural Science Foundation of China (No. 40971124 and No. 41371223), China Scholarship Council (201408210121 and 201508210201), and Science and Technology Department of Liaoning Province (Liaoning Province Doctoral Startup Fund: No. 20170520407) for their financial support for this project. Our acknowledgements also extended to the anonymous reviewers for their constructive reviews of the manuscript.

Reference

An, Z.S., Kukla, G., Porter, S.C., Xiao, J.L., 1991. Late Quaternary dust flow on the Chinese loess plateau. Catena 18 (2), 125–132.

Bahlburg, H., Dobrzinski, N., 2011. Chapter 6 a review of the Chemical Index of Alteration (CIA) and its application to the study of Neoproterozoic glacial deposits and climate transitions. Geol. Soc. Lond. Mem. 36, 81–92.

Bokhorst, M.P., Beets, C.J., Marković, S.B., Gerasimenko, N.P., Matviishina, Z.N., Frechen, M., 2009. Pedo-chemical climate proxies in Late Pleistocene Serbian–Ukranian loess sequences. Quat. Int. 198, 113–123.

Brasher, B.R., Franzmeier, D.P., Valassis, V., Davidson, S.E., 1966. Use of saran resin to coat natural soil clods for bulk density and water retention measurements. Soil Sci. 101, 108.

Brewer, R., 1976. Fabric and Mineral Analysis. Robert E. Krieger Publishing Company, New York.

Buggle, B., Glaser, B., Hambach, U., Gerasimenko, N., Marković, S., 2011. An evaluation

of geochemical weathering indices in loess–paleosol studies. Quat. Int. 240, 12–21.
Buggle, B., Glaser, B., Zöller, L., Hambach, U., Marković, S., Glaser, I., Gerasimenko, N., 2008. Geochemical characterization and origin of Southeastern and Eastern European loesses (Serbia, Romania, Ukraine). Quat. Sci. Rev. 27, 1058–1075.
Buggle, B., Hambach, U., Glaser, B., Gerasimenko, N., Marković, S., Glaser, I., Zöller, L., 2009. Stratigraphy, and spatial and temporal paleoclimatic trends in Southeastern/Eastern European loess–paleosol sequences. Quat. Int. 196, 86–106.
Cesareo, R., 2010. X-Ray Fluorescence Spectrometry. Wiley Online Library.
Chen, H., 2009. Grain-Size Characteristics and Paleoclimatic Reconstruction During the Late Middle Pleistocene and the Last Interglacial Stage of a Paleosol Sequence at Fenghuang Mountain in Chaoyang, Liaoning Province (In Chinese). College of Land and Environment. Shenyang Agricultural University.
Chen, H., Wang, Q.B., Han, C.L., Wu, D.L., 2009. Grain-size distribution and material origin of a paleosol sequence at Fenghuang Mountain, Chaoyang, Liaoning Province. Earth and Environment 37, 243–248.
Chen, J., An, Z.S., Head, J., 1999. Variation of Rb/Sr ratios in the loess-paleosol sequences of central China during the last 130,000 years and their implications for monsoon paleoclimatology. Quat. Res. 51, 215–219.
Condie, K.C., 1993. Chemical composition and evolution of the upper continental crust: contrasting results from surface samples and shales. Chem. Geol. 104, 1–37.
Dasch, E.J., 1969. Strontium isotopes in weathering profiles, deep-sea sediments, and sedimentary rocks. Geochim. Cosmochim. Acta 33, 1521–1552.
Ding, Z.L., Sun, J.M., Yang, S.L., Liu, T.S., 2001. Geochemistry of the Pliocene red clay formation in the Chinese Loess Plateau and implications for its origin, source provenance and paleoclimate change. Geochim. Cosmochim. Acta 65, 901–913.
Ding, Z.L., Xiong, S.F., Sun, J.M., Yang, S.L., Gu, Z.Y., Liu, T.S., 1999. Pedostratigraphy and paleomagnetism of a ~7.0 Ma eolian loess-red clay sequence at Lingtai, Loess Plateau, north-central China and the implications for paleomonsoon evolution. Palaeogeogr. Palaeoclimatol. Palaeoecol. 152, 49–66.
Duzgoren-Aydin, N., Aydin, A., Malpas, J., 2002. Re-assessment of chemical weathering indices: case study on pyroclastic rocks of Hong Kong. Eng. Geol. 63, 99–119.
Egli, M., Fitze, P., Mirabella, A., 2001. Weathering and evolution of soils formed on granitic, glacial deposits: results from chronosequences of Swiss alpine environments. Catena 45, 19–47.
Egli, M., Mirabella, A., Sartori, G., Fitze, P., 2003. Weathering rates as a function of climate: results from a climosequence of the Val Genova (Trentino, Italian Alps). Geoderma 111, 99–121.
Essington, M.E., 2004. Soil and Water Chemistry: An Integrative Approach. CRC Press.
Fedo, C.M., Nesbitt, H.W., Young, G.M., 1995. Unraveling the effects of potassium metasomatism in sedimentary rocks and paleosols, with implications for paleoweathering conditions and provenance. Geology 23, 921–924.
Gallet, S., Jahn, B.-M., Torii, M., 1996. Geochemical characterization of the Luochuan loess-paleosol sequence, China, and paleoclimatic implications. Chem. Geol. 133, 67–88.
Garrels, R.M., Mackenzie, F.T., 1967. Origin of the Chemical Compositions of Some Springs and Lakes. Vol. 67. pp. 222–242.
Garrels, R.M., Mackenzie, F.T., 1971. Evolution of Sedimentary Rocks. Norton & Company, New York.
Gu, Z.Y., Ding, Z.L., Xiong, S.F., Liu, T.S., 1999. A seven million geochemical record from chinese red-clay and loess-paleosol sequence: weathering and erosion in northwestern china. Quaternary Sciences 4, 007.
Guo, Z.T., Biscaye, P.E., Wei, L.Y., Chen, X.H., Peng, S.Z., Liu, T.S., 2000. Summer monsoon variations over the last 1.2 Ma from the weathering of loess–soil sequences in China. Geophys. Res. Lett. 27, 1751–1754.
Harden, J.W., 1982. A quantitative index of soil development from field descriptions: examples from a chronosequence in central California. Geoderma 28, 1–28.
Harden, J.W., Taylor, E.M., 1983. A quantitative comparison of soil development in four climatic regimes. Quat. Res. 20, 342–359.
Harnois, L., 1988. The CIW index: a new chemical index of weathering. Sediment. Geol. 55, 319–322.
Hawkesworth, C.J., Kemp, A.I., 2006. Evolution of the continental crust. Nature 443, 811–817.
Helgeson, H.C., Garrels, R.M., Mackenzie, F.T., 1969. Evaluation of irreversible reactions in geochemicai processes involving minerals and aqueous solutions-II applications. Geochim. Cosmochim. Acta 33, 455–481.
Heller, F., Tungsheng, L., 1984. Magnetism of Chinese loess deposits. Geophys. J. Int. 77, 125–141.
Kronberg, B., Nesbitt, H., 1981. Quantification of weathering, soil geochemistry and soil fertility. J. Soil Sci. 32, 453–459.
Li, X.S., H, Z.Y., Yang, S.Y., Chen, Y.Y., Wang, Y.B., Yang, D.Y., 2007. Chemical weathering intensity and element migration features of the Xiashu Loess profile in Zhenjiang (in Chinese). Acta Geograph. Sin. 62, 1174–1184.
Liu, T.S., 1985. Loess and the Environment. China Ocean Press, Beijing.
Liu, T.S., Guo, Z.T., Liu, J.Q., Han, J.M., Ding, Z.L., Gu, Z.Y., Wu, N.Q., 1995. Variations of eastern Asian monsoon over the last 140,000 years. Bull. Soc. Geol. Fr. 166, 221–229.
Loughnan, F.C., 1969. Chemical Weathering of the Silicate Minerals. Elsevier, New York.
Mason, B., Moore, C.B., 1985. Principles of Geochemistry, 4th ed. John Wiley & Sons Inc., Canada.
McLennan, S.M., 1993. Weathering and global denudation. The J. Geol. 101, 295–303.
National Geographic World Map, 2010. National Geographic, E., Delorme, HERE, UNEP-WCMC, USGS, NASA, ESA, METI, NRCAN, GEBCO, NOAA, increment P Corp.
Nesbitt, H., Young, G., 1982. Early Proterozoic climates and plate motions inferred from major element chemistry of lutites. Nature 299, 715–717.
Nesbitt, H., Young, G., 1984. Prediction of some weathering trends of plutonic and volcanic rocks based on thermodynamic and kinetic considerations. Geochim. Cosmochim. Acta 48, 1523–1534.
Nesbitt, H., Young, G., McLennan, S., Keays, R., 1996. Effects of chemical weathering and sorting on the petrogenesis of siliciclastic sediments, with implications for provenance studies. The J. Geol. 525–542.
Nesbitt, H., Young, G.M., 1989. Formation and diagenesis of weathering profiles. The J. Geol. 129–147.
Nesbitt, H.W., Markovics, G., 1980. Chemical processes affecting alkalis and alkaline earths during continental weathering. Geochim. Cosmochim. Acta 44, 1659–1666.
Nicholls, G., 1963. Environmental studies in sedimentary geochemistry. Sci. Prog. 51, 12–31 (1933-).
Parker, A., 1970. An index of weathering for silicate rocks. Geol. Mag. 107, 501–504.
Roy, P.D., Arce, J.L., Lozano, R., Jonathan, M., Centeno, E., Lozano, S., 2012. Geochemistry of Late Quaternary tephra-sediment sequence from north-eastern Basin of Mexico (Mexico): implications to tephrochronology, chemical weathering and provenance. Revista Mexicana de Ciencias Geológicas 29, 24–38.
Rudnick, R.L., Gao, R., 2003. Composition of the continental crust. In: Rudnick, R.L. (Ed.), The Crust. Elsevier, Amsterdam, pp. 1–64.
Schaetzl, R.J., Anderson, S., 2005. Soils: Genesis and Geomorphology. Cambridge University Press, New York.
Schellenberger, A., Veit, H., 2006. Pedostratigraphy and pedological and geochemical characterization of Las Carreras loess–paleosol sequence, Valle de Tafí, NW-Argentina. Quat. Sci. Rev. 25, 811–831.
Schoeneberger, P.J., Wysocki, D.A., Benham, E.C., Soil-Survey-Staff, 2012. Field Book for Describing and Sampling Soils, Version 3.0. Natural Soil Survey Center, Lincoln, NE.
Sheldon, N.D., Retallack, G.J., Tanaka, S., 2002. Geochemical climofunctions from North American soils and application to paleosols across the Eocene–Oligocene boundary in Oregon. The J. Geol. 110, 687–696.
Smeck, N.E., Wilding, L.P., 1980. Quantitative evaluation of pedon formation in calcareous glacial deposits in Ohio. Geoderma 24, 1–16.
Soil Survey Staff, 2014. Keys to soil taxonomy, 12th ed.[1] USDA, NRCS. U.S. Gov. Print. Office, Washington, DC.
Sun, Z.-X., Owens, P.R., Han, C.-L., Chen, H., Wang, X.-L., Wang, Q.-B., 2016. A quantitative reconstruction of a loess–paleosol sequence focused on paleosol genesis: an example from a section at Chaoyang, China. Geoderma 266, 25–39.
Sun, Z.-X., Wang, Q.-B., Han, C.-L., Zhang, Q.-J., Owens, P.R., 2016. Clay mineralogical characteristics and the palaeoclimatic significance of a Holocene to Late Middle Pleistocene loess–palaeosol sequence from Chaoyang, China. Earth and Environmental Science Transactions of the Royal Society of Edinburgh 1–13.
Tan, W.F., Liu, F., Li, Y.H., Hu, H.Q., Huang, Q.Y., 2006. Elemental composition and geochemical characteristics of iron-manganese nodules in main soils of China. Pedosphere 16, 72–81.
Yang, S.L., Ding, F., Ding, Z.L., 2006. Pleistocene chemical weathering history of Asian arid and semi-arid regions recorded in loess deposits of China and Tajikistan. Geochim. Cosmochim. Acta 70, 1695–1709.